Article

Neural Network Based Control of Four-Bar Mechanism with Variable Input Velocity

R. Peón-Escalante [ID], Manuel Flota-Bañuelos [ID], Roberto Quintal-Palomo *[ID], Luis J. Ricalde [ID], F. Peñuñuri [ID], B. Cruz Jiménez and J. Avilés Viñas [ID]

Faculty of Engineering, University of Yucatan, Mérida 97000, Mexico
* Correspondence: roberto.quintal@correo.uady.mx

Abstract: For control applications, the angular velocity of the drive crank of a four-bar mechanism is traditionally assumed to be constant. In this paper, we propose control of variable velocity of the drive crank to obtain the desired output motions for the coupler point. To estimate the reference trajectory for the crank velocity, a neural network is trained with data from the kinematic model. The control law is designed from feedback linearization of the tracking error dynamics and a Proportional–Integral–Derivative (PID) controller. The applicability of the proposed scheme is validated through simulations for three variable speed profiles, obtaining excellent results from the system.

Keywords: four-bar mechanism; variable input-velocity; trajectory tracking; PID neural network controller

MSC: 70E60

1. Introduction

When an electric motor is coupled in a four-bar mechanism, a periodically time varying torque, produced by the changing inertia of the mechanism during its rotation, is applied as an external load to the motor [1]. Different control techniques have been studied to regulate the crank angular velocity fluctuations introduced by the inertia of the rotor and the rotating bars in four-bar linkages. Among applied controllers that address this issue, are proportional–integral–derivative (PID) [1], proportional–derivative (PD) [2–4], nonlinear PD [5], model reference adaptive control [6], fuzzy [7], type-2 fuzzy sliding mode [8], adaptive fuzzy sliding mode [9], robust fuzzy [10], PID Fuzzy [11], PID neural network [12], PD and neural adaptive [13], moving sliding mode [14], robust backstepping control [15], and fuzzy logic controller combined with grey system modeling approach [16]. In [17], several control schemes are investigated (filtered proportional–integral–derivative, filtered sliding mode, filtered fuzzy, and filtered genetic-based reinforcement neuro-controller). In reference [18], experimental data were used to develop parametric models for a four-bar mechanism driven by a geared DC motor by employing artificial neural networks. In reference [19], PID linear control was used to control a micro-aerial-vehicle that has four flapping wings (four-bar mechanisms). In [20], the gains of a PID controller for the four-bar mechanism are optimized via evolutionary algorithms. Recently, in [21], an indirect adaptive control based on online multi-objective optimization for the velocity regulation of the four-bar mechanism was proposed. Other advanced control schemes for trajectory tracking in mechanical systems consider sliding modes [22] and Linear Matrix Inequalities (LMI) approaches [23], which are both applied for docking mechanisms. Furthermore, optimal sliding mode control has been applied in quick-return mechanisms [24]. On the other hand, fuzzy-based controlled schemes for trajectory tracking have been recently developed with applications on mobile robots with promising results [25–27]. In reference [25], the design of a highly efficient path-following scheme for wheeled mobile robots is proposed. Here the authors present a new controller constructed by the type-3 (T3) fuzzy logic systems (FLS) and a predictive compensator where the stability of the complete system is validated with

the Lyapunov methodology. Furthermore, this scheme is tested with good performance in a chaotic generated path.

The main topic of this work is to integrate computational intelligence methods to solve the inverse kinematics problem to control a four-bar mechanism for trajectory tracking in the coupler point; this trajectory requires a variable angular velocity of the drive crank. This control scheme is defined as variable input velocity control. There are few reports of simulation studies on cases of trajectory tracking where the problem of variable input velocity control is addressed [2,3,6,15,28–30]. In [6], a model reference adaptive controller for the velocity regulation of a four-bar mechanism is designed. In reference [2], motion control of four-bar mechanism driven by a brushless servo motor is applied where simulation and experimental results were validated for different crank motion profiles. In [3], a PD control algorithm is employed for trajectory tracking in a four-bar mechanism which is redesigned by applying a new mass-distribution scheme. In reference [28], an integrated approach for variable input velocity servo four-bar linkages is designed in order to satisfy the kinematic requirements, reduce the shaking force and moment, improve the velocity trajectory tracking performance, and minimize the motor power dissipation where dimensions of the links, counterweights, input-velocity trajectory and controller parameters are considered as design variables simultaneously. In [15], a robust backstepping controller is designed and tested in simulation for a four-bar linkage mechanism that is driven by a DC motor, without a priori knowledge of the model parameters where five cases were examined. In reference [29,30], the problem of trajectory tracking by controlling the angular velocity of the input link is investigated in a four-bar mechanism to fulfill moving the coupler point with a constant velocity. A vision controller for regulation of the velocity of the coupler point in a four-bar mechanism was implemented in [30], where the desired trajectory for the coupler point of the mechanism is achieved by controlling the angular velocity of the crank using a feedback linearization algorithm for the error dynamics and a PID controller.

For a four-bar mechanism, the characteristics of the output movement depend on the crank's input movement. Then, it is necessary that the designed control fulfills the mechanism desired input velocity profile in order for the output motion to follow the desired trajectory. In this work, the problem of trajectory tracking is considered; the variable input velocity control is designed to ensure that the coupler point follows a constant velocity reference. To obtain the reference for the crank velocity and to reduce the computational burden for the synthesized control, a neural network is implemented. Neural networks have been widely applied to aid the control design process for mechanisms due to their simple design and easy implementation. In [12], a feed-forward neural network is applied to predict the reference model used by a PID controller for the constant velocity of the crank.

The structure of this work is presented as follows: Section 2 explains the kinematic model for the four-bar mechanism, the DC motor and mechanical coupling mathematical models are developed, and the overall dynamic model is presented. In Section 3, the Artificial Neural Network and PID control scheme are synthesized. Section 4 presents the path for the coupler point in the mechanism, and simulation results for several cases of trajectory tracking are discussed. In Section 5, the conclusions are summarized.

2. Mathematical Model for a Motor-Driven Four-Bar Mechanism System

2.1. Dynamics of the Four-Bar Linkages

A general four-bar linkage is presented in Figure 1, where link L_2 (crank) is driven by an electrical motor, and it is able to perform a complete rotation. The link L_3 (coupler) performs a general motion in the plane, and it transmits the movement to link L_4 (rocker), which executes an oscillatory motion, and the link L_1 (ground) is fixed with respect to the reference frame. The kinematic model of the four-bar mechanism is defined with respect to the global reference system $\{X - Y\}$. The local reference system $\{x_r - y_r\}$ is assigned with the origin coinciding on the pivot O_2 of the mechanism and is specified the direction x_r along of the link L_1. Thus, the relation between the local reference system with respect to the global $\{X - Y\}$, is defined by the translation r_0 and orientation α.

The parameters in Figure 1 required to develop the dynamical model of the mechanism are summarized in Table 1. Each link has a mass of m_i, a mass moment of inertia with respect to the centroid J_i, and L_i is the length of the link i. The angular positions of each link with respect to the x_r axis of the base frame are denoted by ϕ_2, ϕ_3, and ϕ_4. The position vector of the center of mass for each link i is displayed by a dark circle and their locations are described by r_i and θ_i. A torsional spring with a stiffness constant k_s and a torsional damper with a damping constant c are attached to the rocker link to represent a general loading situation.

Table 1. Parameters of four-bar mechanism.

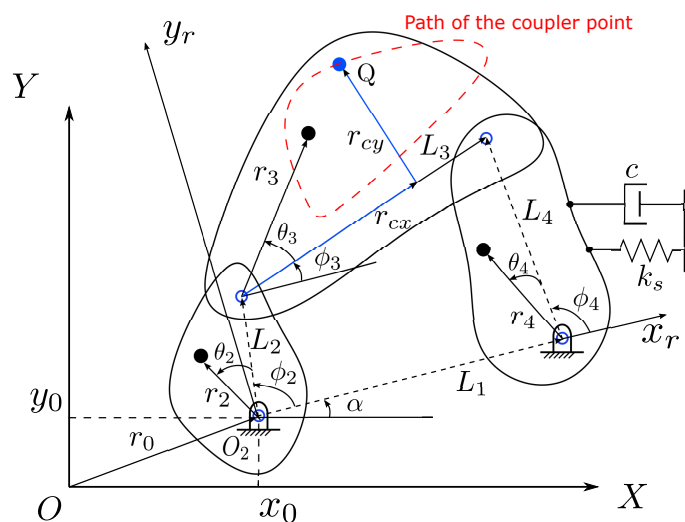| Parameter	Description for Each Link
L_i	length of the link i
ϕ_i	angular position for link i with respect to the axis x_r
m_i	mass of link i
J_i	mass moment of inertia
r_i and θ_i	location of the center of mass for each link i
r_{cx} and r_{cy}	location of point Q on link 3

Figure 1. Schematic of four-bar linkage.

Applying the Euler–Lagrange modeling methodology [1,31], the equation of motion for the mechanism, by using the crank angle ϕ_2 as the generalized coordinate, is given by

$$\frac{d}{dt}\left(\frac{\partial K}{\partial \dot{\phi}_2}\right) - \frac{\partial K}{\partial \phi_2} + \frac{\partial P}{\partial \phi_2} + \frac{\partial D}{\partial \dot{\phi}_2} = T \tag{1}$$

where K, P, and D denote the kinetic, potential, and dissipative energies, respectively, and T is the applied external torque. The dissipation term can be neglected in the mechanism, since the damping is relatively small.

The kinetic energy of the mechanism is defined as

$$K = \sum_{i=2}^{4}\left[\frac{1}{2}m_i(V_{ix}^2 + V_{iy}^2) + \frac{1}{2}J_i\dot{\phi}_i^2\right] \tag{2}$$

where V_{ix} and V_{iy} represent the components of velocity at the mass center in X and Y of the link i, and $\dot{\phi}_i$ is the angular velocity of the link i.

According to the scheme in Figure 1, the kinetic energy can be expressed as

$$K = \frac{1}{2} A(\phi_2) \dot{\phi}_2^2 \tag{3}$$

where $A(\phi_2)$ is defined as,

$$A(\phi_2) = C_0 + C_1 \gamma_3^2 + C_2 \gamma_4^2 + C_3 \gamma_3 \cos(\phi_2 - \phi_3 - \theta_3) \tag{4}$$

and

$$C_0 = J_2 + m_2 r_2^2 + m_3 L_2^2$$
$$C_1 = J_3 + m_3 r_3^2$$
$$C_2 = J_4 + m_4 r_4^2$$
$$C_3 = 2 L_2 r_3 m_3$$

From the four-bar linkage kinematics analysis position, the functions for the angular position of the coupler link, ϕ_3, and the oscillator link, ϕ_4, are determined.

The angle ϕ_3, corresponding to the orientation for coupler link, L_3, is defined from

$$\phi_3(\phi_2) = 2 \arctan\left(\frac{-k_b \pm \sqrt{k_b^2 - 4 k_a k_c}}{2 k_a} \right) \tag{5}$$

where

$$k_a = -l_1 + (l_2 + 1) \cos\phi_2 + l_3,$$
$$k_b = -2 \sin\phi_2,$$
$$k_c = l_1 + (l_2 - 1) \cos\phi_2 + l_3,$$

and the constants l_1, l_2, and l_3 are

$$l_1 = \frac{L_1}{L_2}$$
$$l_2 = \frac{L_1}{L_3}$$
$$l_3 = \frac{L_4^2 - L_1^2 - L_2^2 - L_3^2}{2 L_2 L_3}$$

The angle ϕ_4, corresponding to the orientation for oscillator link L_4, is defined from

$$\phi_4(\phi_2) = 2 \arctan\left(\frac{-k_b \pm \sqrt{k_b^2 - 4 k_d k_e}}{2 k_d} \right) \tag{6}$$

where the coefficients k_d and k_e are

$$k_d = -l_1 + (1 - l_4) \cos\phi_2 + l_5,$$
$$k_e = l_1 - (l_4 + 1) \cos\phi_2 + l_5,$$

and the constants l_4 and l_5 are

$$l_4 = \frac{L_1}{L_4}$$
$$l_5 = \frac{L_2^2 - L_3^2 + L_4^2 + L_1^2}{2 L_2 L_4}.$$

From four-bar linkage kinematics analysis, the functions for the angular velocity of the coupler link, $\dot{\phi}_3$ can be expressed as

$$\dot{\phi}_3 = \gamma_3\,\dot{\phi}_2 \tag{7}$$

where γ_3 is defined as

$$\gamma_3 = \frac{L_2\sin(\phi_4 - \phi_2)}{L_3\sin(\phi_3 - \phi_4)}$$

and the angular velocity of the rocker link, $\dot{\phi}_4$ is

$$\dot{\phi}_4 = \gamma_4\,\dot{\phi}_2 \tag{8}$$

where γ_4 is defined as

$$\gamma_4 = \frac{L_2\sin(\phi_3 + \phi_2)}{L_4\sin(\phi_3 - \phi_4)}$$

It is important to notice that from (7) and (8), both $\dot{\phi}_3$ and $\dot{\phi}_4$ are functions of the crank link-driven velocity $\dot{\phi}_2$, which is the time derivative of the generalized coordinate.

The first term of the Euler–Lagrange movement equation is

$$\frac{d}{dt}\left(\frac{\partial K}{\partial \dot{\phi}_2}\right) = \frac{dA(\phi_2)}{d\phi_2}\dot{\phi}_2^2 + A(\phi_2)\ddot{\phi}_2 \tag{9}$$

Then, the second term of (1), yields

$$\frac{\partial K}{\partial \phi_2} = \frac{1}{2}\frac{dA(\phi_2)}{d\phi_2}\dot{\phi}_2^2 \tag{10}$$

In order to determine $\dfrac{dA(\phi_2)}{d\phi_2}$, it is necessary to calculate $\dfrac{d\gamma_3}{d\phi_2}$ and $\dfrac{d\gamma_4}{d\phi_2}$

The term $\dfrac{d\gamma_3}{d\phi_2}$ can be obtained from

$$\frac{d\gamma_3}{d\phi_2} = \frac{L_2}{L_3}\left[\frac{D_1 + D_2}{\sin^2(\phi_3 - \phi_4)}\right] \tag{11}$$

where

$$D_1 = (\gamma_4 - 1)\cos(\phi_4 - \phi_2)\sin(\phi_3 - \phi_4)$$
$$D_2 = (\gamma_4 - \gamma_3)\sin(\phi_4 - \phi_2)\cos(\phi_3 - \phi_4)$$

The term $\dfrac{d\gamma_4}{d\phi_2}$ is expressed as

$$\frac{d\gamma_4}{d\phi_2} = \frac{L_2}{L_4}\left[\frac{D_3 + D_4}{\sin^2(\phi_3 - \phi_4)}\right] \tag{12}$$

where

$$D_3 = (\gamma_3 - 1)\cos(\phi_3 - \phi_2)\sin(\phi_3 - \phi_4)$$
$$D_4 = (\gamma_4 - \gamma_3)\sin(\phi_3 - \phi_2)\cos(\phi_3 - \phi_4)$$

Using the expressions (11) and (12), we can rewrite $\dfrac{dA(\phi_2)}{d\phi_2}$ as

$$\frac{dA(\phi_2)}{d\phi_2} = \frac{L_2}{L_3}\left[\frac{D_1 + D_2}{\sin^2(\phi_3 - \phi_4)}\right][2C_1\gamma_3 + C_3\cos(\phi_2 - \phi_3 - \theta_3)] + 2\,C_2\gamma_4\frac{L_2}{L_4}\left[\frac{D_3 + D_4}{\sin^2(\phi_3 - \phi_4)}\right]$$
$$+ C_3\gamma3[-\sin(\phi_2 - \phi_3 - \theta_3)(1 - \gamma_3)] \tag{13}$$

To obtain the term $\frac{\partial P}{\partial \phi_2}$, let us consider that the potential energy from the four-bar mechanism can be expressed as

$$P = P_g + P_s \tag{14}$$

where P_g indicates the potential energy caused by gravity and P_s is the potential energy stored in the torsional spring. The potential energy due to gravitational forces can be expressed as

$$P_g = [m_2 r_2 \sin(\theta_2 + \phi_2) + m_3(L_2 \sin\phi_2 + r_3 \sin(\theta_3 + \phi_3))$$
$$+ m_4(L_1 \sin\theta_1 + r_4 \sin(\phi_4 + \theta_4))]g$$

Now, taking the time derivative of the potential energy with respect to ϕ_2, it follows

$$\frac{\partial P_g}{\partial \phi_2} = [m_2 r_2 \cos(\theta_2 + \phi_2) + m_4(r_4\gamma_4 \cos(\theta_4 + \phi_4))$$
$$+ m_3(L_2 \cos\phi_2 + r_3\gamma_3 \cos(\theta_3 + \phi_3))]g \tag{15}$$

The potential energy stored in the torsional spring can be written as

$$P_s = \frac{1}{2}k(\phi_4 - \phi_{4,0})^2 \tag{16}$$

and the dissipation energy is given by

$$D = \frac{1}{2}c\dot{\phi}_4^2 \tag{17}$$

Differentiating Equation (16) with respect to ϕ_2, and (17) with respect to $\dot{\phi}_2$, and using (8) we have

$$\frac{\partial P_s}{\partial \phi_2} = k_s\,\gamma_4(\phi_4 - \phi_{4,0}) \tag{18}$$

$$\frac{\partial D}{\partial \dot{\phi}_2} = C\gamma_4^2\dot{\phi}_2 \tag{19}$$

To this end, the motion equation can be written by employing (9), (10), (15), (18), and (19) as

$$A(\phi_2)\ddot{\phi}_2 + \frac{1}{2}\frac{dA(\phi_2)}{d\phi_2}\dot{\phi}_2^2 + k\,\gamma_4(\phi_4 - \phi_{4,0}) + c\gamma_4^2\dot{\phi}_2 + [m_2 r_2 \cos(\theta_2 + \phi_2)$$
$$+ m_4(r_4\gamma_4 \cos(\theta_4 + \phi_4))m_3(L_2 \cos\phi_2 + r_3\gamma_3 \cos(\theta_3 + \phi_3))]g = T \tag{20}$$

2.2. Mathematical Model of the Electric Motor and Transmission

In Figure 2, a schematic diagram of the electric motor is presented. The transmission ratio is

$$n = \frac{T_b}{T_a} = \frac{\omega_a}{\omega_b} \tag{21}$$

where ω_a and T_a are the angular speed and the torque at the shaft a, respectively, ω_b is the angular velocity of the shaft b. T_b is the system-delivered torque and is equal to T in Equation (1).
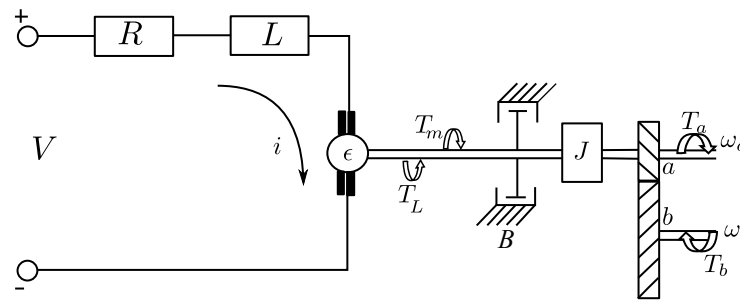
Figure 2. Schematic diagram of the motor and transmission.

By using Kirchoff's voltage law we obtain

$$V_a = Ri(t) + L\dot{i}(t) + e \tag{22}$$

where V_a is the input voltage to the motor–gear system, R is the motor's armature resistance, L is the motor inductance, $i(t)$ is the current, and e is the electromotive force generated by the motor. The applied torques in the motor and gear are expressed as

$$T = n(T_m - T_L - B\omega_a - J\dot{\omega}_a) \tag{23}$$

where T_m represents the motor electromagnetic torque and n is the transmission ratio defined in Equation (21).

The magnetic torque and the back electromotive force are defined as

$$T_m = K_m i(t) \tag{24}$$
$$e = K_g \omega_a \tag{25}$$

where K_m and K_g represent the torque and voltage parameters of the motor.

Since the shaft b gives propulsion to the crank mechanism, (21) can be written as:

$$\omega_a = n\omega_b = n\dot{\phi}_2 \tag{26}$$

From (22)–(26), the mathematical model of the motor is obtained as

$$\dot{i}(t) = \frac{1}{L}(V_a - Ri(t) - nK_g\dot{\phi}_2) \tag{27}$$
$$T = nK_m i(t) - nT_L - n^2 B\dot{\phi}_2 - n^2 J\ddot{\phi}_2 \tag{28}$$

2.3. Dynamic Model of the System

The potential and dissipative energies can be neglected in the mechanism since they are relatively small and the terms related to potential energy and due to the orientation of the mechanism. In this way, combining (20) and (28), the nonlinear equation of the system movement is

$$A(\phi_2)\ddot{\phi}_2 + \frac{1}{2}\frac{dA(\phi_2)}{d\phi_2}\dot{\phi}_2^2 = nK_m i(t) - nT_L - n^2 B\dot{\phi}_2 - n^2 J\ddot{\phi}_2 \tag{29}$$

From (27) and (29), it is possible to present the complete system model in state space as

$$\frac{d}{dt}\left(\frac{d\phi_2}{dt}\right) = A_0\left[A_1\left(\frac{d\phi_2}{dt}\right)^2 + A_2\frac{d\phi_2}{dt} + nK_m i + A_3\right] \tag{30}$$
$$\frac{di}{dt} = \frac{1}{L}\left(V_a - Ri - nK_g\frac{d\phi_2}{dt}\right) \tag{31}$$

where

$$A_0 = \frac{1}{A(\phi_2) + n^2 J}$$

$$A_1 = -\frac{1}{2}\frac{A(\phi_2)}{\phi_2}$$

$$A_2 = -n^2 B$$

$$A_3 = -n T_L$$

3. ANN-Based PID Control Scheme

The control scheme described in this work consists of two stages. The first one obtains the current reference (i_a), which is a virtual control signal as a function of the velocity error. The second stage determines the armature voltage applied to the motor (v_a), which is necessary to achieve the desired coupler point velocity. Linearization via feedback and a PID controller are applied in both control loops to assure the correct velocity regulation in the coupler point. It is important to highlight that for each point of the trajectory, it is necessary to solve the kinematic model for the crank velocity for the coupler point motion to reach the desired speed. A neural network estimator is used for this task as a variable velocity drive estimator. The complete control scheme is presented in Figure 3.
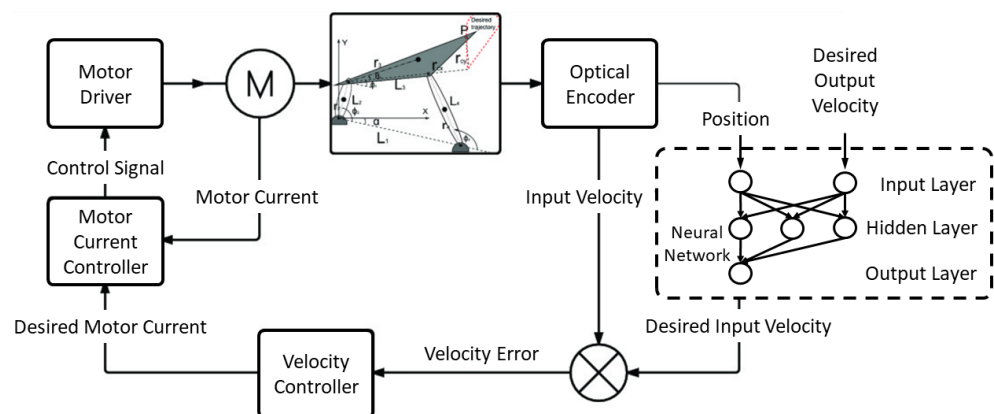

Figure 3. ANN-based control scheme for variable input velocity tracking of four-bar mechanism.

3.1. Current Control Loop

To synthesize the control law for the motor current, the tracking error is defined as $e_i = i - i^*$. Taking into account (31), the error dynamics $\frac{de_i}{dt}$ can be written as

$$\frac{de_i}{dt} = \frac{1}{L}\left(V_a - R\,i - n\,k_g\,\dot{\phi}_2\right) - \frac{di^*}{dt}. \tag{32}$$

From (32), a linearizing PID control signal can be proposed as follows:

$$V_a = R\,i + n\,k_g\,\dot{\phi}_2 + L\,\frac{di^*}{dt} - L\left(k_p\,e_i + k_i\,\eta + k_d\,\frac{de_i}{dt}\right) \tag{33}$$

where

$$\frac{d\eta}{dt} = e_i$$

Introducing the control law (33) into the error dynamics (32), we obtain

$$\begin{aligned}\frac{de_i}{dt} &= -k_p\,e_i - k_i\,\eta - k_d\,\frac{de_i}{dt} \\ &= -\frac{k_p\,e_i + k_i\,\eta}{1 + k_d}\end{aligned} \tag{34}$$

where the error dynamics can be globally asymptotically stable if the gains k_p, k_i, and k_d are adequately selected.

3.2. Velocity Control Loop

As can be noted, the control law (33), includes the current reference (i^*) and its time derivative. To calculate this reference signal, we design the second control loop where we must consider the velocity tracking error, defined as $e_v = \dot{\phi}_2 - \dot{\phi}_2^*$, where $\dot{\phi}_2^*$ is the reference velocity. Considering (30), the velocity error dynamics can be written as

$$\frac{de_v}{dt} = A_0 \left(A_1 \dot{\phi}_2^{\,2} + A_2 \dot{\phi}_2 + n K_m i + A_3 \right) - \frac{d}{dt} \dot{\phi}_2^*. \tag{35}$$

Replacing i with $e_i + i^*$,

$$\frac{de_v}{dt} = A_0 \left(A_1 \dot{\phi}_2^{\,2} + A_2 \dot{\phi}_2 + n K_m \left(e_i + i^* \right) + A_3 \right) - \frac{d}{dt} \dot{\phi}_2^*. \tag{36}$$

Taking into account that the first control loop ensures that $e_i \to 0$ in short time, (36) is reduced to

$$\frac{de_v}{dt} = A_0 \left(A_1 \dot{\phi}_2^{\,2} + A_2 \dot{\phi}_2 + n K_m i^* + A_3 \right) - \frac{d}{dt} \dot{\phi}_2^*. \tag{37}$$

As i^* is considered a virtual control signal, it can be proposed as

$$i^* = -\frac{1}{n\, k_m} \left(A_1 \dot{\phi}_2^{\,2} + A_2 \dot{\phi}_2 + A_3 + \frac{k_{p2}\, e_v + k_{i2}\, \xi + k_{d2} \dfrac{de_v}{dt} - \dfrac{d}{dt}\dot{\phi}_2^*}{A_0} \right), \tag{38}$$

where

$$\dot{\xi} = e_v.$$

Then, replacing the control law (38) into the velocity error dynamics (37), we obtain

$$\begin{aligned} d\frac{e_v}{dt} &= -k_{p2}\, e_v - k_{i2}\, \xi - k_{d2}\, d\frac{e_v}{dt} \\ &= -\frac{k_{p2}\, e_v + k_{i2}\, \xi}{1 + k_{d2}}. \end{aligned} \tag{39}$$

To verify the stability of the complete closed loop system, a Lyapunov candidate function is proposed as

$$W(z) = z^T K z > 0 \tag{40}$$

where

$$z = [e_i,\ e_v,\ \eta,\ \xi]^T$$

and

$$K = \begin{bmatrix} 1 + k_{d2} & 0 & 1 + k_{d2} & 0 \\ 0 & 1 + k_d & 0 & 1 + k_d \\ 1 + k_{d2} & 0 & k_{p2} + k_{i2} & 0 \\ 0 & 1 + k_d & 0 & k_p + k_i \end{bmatrix}$$

Selecting $k_p + k_i > 1 + k_d > 0$ and $k_{p2} + k_{i2} > 1 + k_{d2} > 0$, we can guarantee that the matrix K is positive definite.

Then, if $\dot{W}(z) < 0\ \forall z \in \mathbb{R} - \{0\}$, the global and asymptotically stability condition of the system is demonstrated. So, this time derivative can be written as follows:

$$\begin{aligned} \dot{W}(z) &= \dot{z}^T K z \\ &= -\left(k_{p2} - k_{d2} - 1 \right) e_i^2 - \left(k_p - k_d - 1 \right) e_v^2 - k_{i2} \xi^2 - k_i \eta^2 \end{aligned}$$

The above result satisfies the stability condition if $k_p > 1 + k_d$, $k_{p2} > 1 + k_{d2}$, $k_i > 0$, and $k_{i2} > 0$, then the origin of the error dynamics of the complete closed loop system is the unique stability point, and is global and asymptotically stable.

It is important to remark that in the stability proof, the error $e_i = i - i^*$ was not explicitly included because it is identical to the variable ξ.

3.3. Variable Input Velocity Generator with Artificial Neural Networks (ANNs)

To determine the velocity reference $\dot{\phi}_2{}^*$ at which the crank must rotate so that the coupler point Q reaches the desired velocity, we first establish a kinematics model for the four-bar mechanism.

The description of the position of $^O\mathbf{Q}$ with respect to the global reference system $\{X - Y\}$, from Figure 1, is given by

$$^O\mathbf{Q} = \mathbf{r}_0 + R(\hat{z}, \alpha)^r\mathbf{Q} \tag{41}$$

where $^r\mathbf{Q}$ represents the position of the point Q measured with respect the local reference system, $\mathbf{r}_0$ represents the translation, and $R(\hat{z}, \alpha)$ corresponds to the canonical rotation matrix of an angle α around the $\hat{z}$ axis, between the local reference system $\{x_r - y_r\}$ and the global $\{X - Y\}$. This can be expanded as

$$^O\mathbf{Q} = \begin{bmatrix} ^0Q_x \\ ^0Q_y \end{bmatrix} = \begin{bmatrix} x_0 + L_2\cos(\phi_2 + \alpha) + r_{cx}\cos(\phi_3 + \alpha) - r_{cy}\sin(\phi_3 + \alpha) \\ y_0 + L_2\sin(\phi_2 + \alpha) + r_{cx}\sin(\phi_3 + \alpha) + r_{cy}\cos(\phi_3 + \alpha) \end{bmatrix} \tag{42}$$

The linear velocity of the point $^O\mathbf{Q}$ is obtained from the derivate of Equation (42) as

$$^O\mathbf{V}_Q = \begin{bmatrix} ^0V_x \\ ^0V_y \end{bmatrix} = \begin{bmatrix} -L_2\sin(\phi_2 + \alpha)\dot{\phi}_2 - r_{cx}\sin(\phi_3 + \alpha)\dot{\phi}_3 - r_{cy}\cos(\phi_3 + \alpha)\dot{\phi}_3 \\ L_2\cos(\phi_2 + \alpha)\dot{\phi}_2 + r_{cx}\cos(\phi_3 + \alpha)\dot{\phi}_3 - r_{cy}\sin(\phi_3 + \alpha)\dot{\phi}_3 \end{bmatrix} \tag{43}$$

The function of the linear input velocity profile is defined as

$$\|^O\mathbf{V}_Q\| = \sqrt{^0V_x^2 + {}^0V_y^2} \tag{44}$$

The desired angular velocity profile function is given by

$$\dot{\phi}_2 = \frac{\sqrt{^0V_x^2 + {}^0V_y^2}}{\lambda} \tag{45}$$

where

$$\lambda^2 = L_2^2 + r_{cx}^2\gamma^3 + r_{cy}^2\gamma^3 + 2L_2\gamma_3[r_{cx}\cos(\phi_2 - \phi_3) + r_{cy}\sin(\phi_2 - \phi_3)]$$

To reduce the computational burden in the numerical solution of (45), when estimating $\dot{\phi}_2^*$ we train an artificial neural network feed with the measured crank angular position ϕ_2 and the desired output velocity $^O\mathbf{V}_Q$. Computational intelligence methods have been successfully integrated with control schemes to relax the requirement of knowledge of the system model, consider uncertainties, and incorporate performance criteria. In particular, Artificial Neural Networks (ANNs) are attractive due to their nonlinear function approximation capabilities and simplicity of design and implementation.

A neural network generates a function approximation through a training process. The ANN is composed of an input layer with m inputs, a hidden neurons layer with N neurons, and an output layer with one single neuron as shown in Figure 4. Each hidden neuron is fully connected to the inputs and neurons in the output layer via the adaptable weights w_{Ok} and $w_{I(k,m)}$, and b_m and b_O are the bias terms for each neuron. The function φ is known as the activation function and is usually a sigmoid. In feedforward networks,

the learning algorithm is based on retro-propagation of the approximation error which adapts each weight in the network [32].

$$y = \sum_{k=1}^{N} \left[w_{Ok} \cdot \varphi \left(\sum_{m=1}^{M} w_{I(k,m)} \cdot x_m + b_m \right) + b_O \right]$$
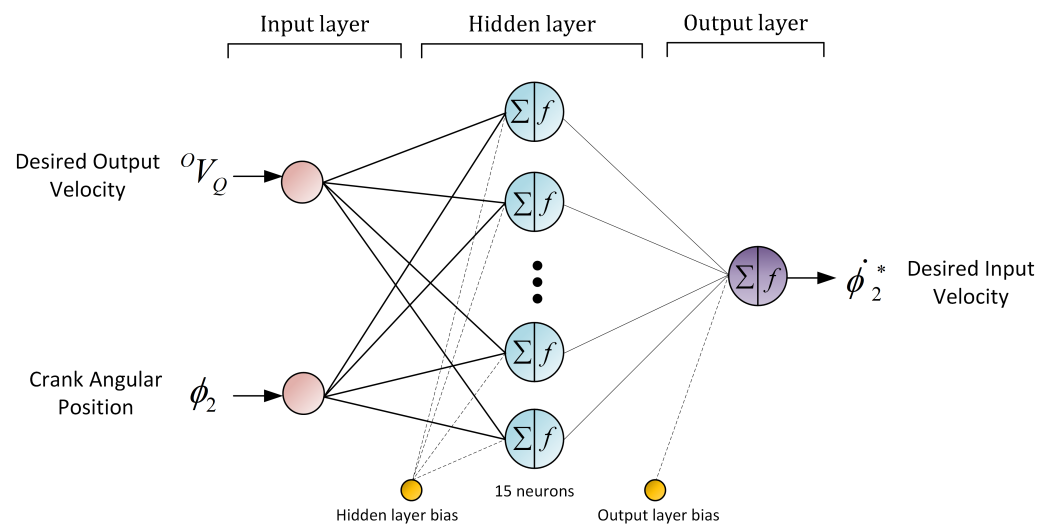
$$\varphi(x) = \frac{1}{1 + e^{-x}}$$

(46)

Figure 4. Neural network estimator for the input velocity Feedforward architecture.

In this study, a two-layer feed-forward neural network with fifteen neurons in its hidden layer was designed. The data to build the neural net were taken by turning the crank at various velocities; the velocity, the coupler point velocity, and the angular position of both were recorded. To adjust the neural network, the crank's angular position and the coupler point's velocity are used as input data; the output data point is the crank velocity. Of the 46 simulation runs under different velocity profiles, 16,560 samples constituted the data set where 70% was used for training, 15% for validation, and 15% for testing. The training algorithm used was Bayesian regularization and the number of epochs is fixed at 1000, with a fitness calculated as $R^2 = 99.99\%$ and a medium square error $MSE = 0.000372$ as displayed in Figure 4.

4. Simulation Results and Discussion

To verify the performance of the proposed control scheme, several simulations in closed-loop were performed. The first simulation applies the state space model of the four-bar mechanism with a PID controller and constant crank velocity. The second test presents the proposed control scheme with a variable input velocity to obtain a constant output velocity at the coupler point. The third experiment presents the proposed control scheme with a variable input velocity, but in this case, it generates two different output velocities at the coupler point. These tests are intended to demonstrate the advantages of the proposed control scheme compared with [28].

4.1. Servo-Controlled Four-Bar Mechanism Simulation Parameters

The parameters of the simulated servo-controlled four-bar mechanism are detailed in Tables 2 and 3. The resulting path of the coupler point for this mechanism is shown in Figure 5. As can be seen, this path has two linear sections followed by two curved segments, the upper one is smooth and the lower one is more demanding. This behavior demonstrates that the relationship between the velocity of the crank and the velocity of the coupler point is nonlinear since the displacements are different, even if the angular

movement is the same. Hence, some points the trajectory generated by the coupler point of the four-bar mechanism have a complex geometric trajectory that will cause abrupt changes in the velocity direction. Therefore, one complex trajectory and the required constant speed profile of the coupler point during the whole trajectory, and limit positions for the output link, evidently will generate speed fluctuations that the controller has to overcome in order to fulfil the task.

Table 2. Mechanism Parameters.

Parameter	Value
L_1 (m)	0.3972
L_2 (m)	0.0588
L_3 (m)	0.2351
L_4 (m)	0.22716
r_{cx} (m)	0.403779
r_{cy} (m)	0.093921
J_2 (kg·m^2)	2.76×10^{-5}
J_3 (kg·m^2)	3.5468×10^{-3}
J_4 (kg·m^2)	3.8779×10^{-4}
m_2 (kg)	0.04234
m_3 (kg)	0.2586
m_4 (kg)	0.08156
α (rad)	5.83047

Table 3. Motor Parameters.

Parameter	Value
R (Ω)	2
L(H)	1
K_m (N·m/A)	0.260
K_g (V·s)	0.260
J (kg·m^2)	0.011
T_L (N·m)	0.28
B (N·m·s)	0
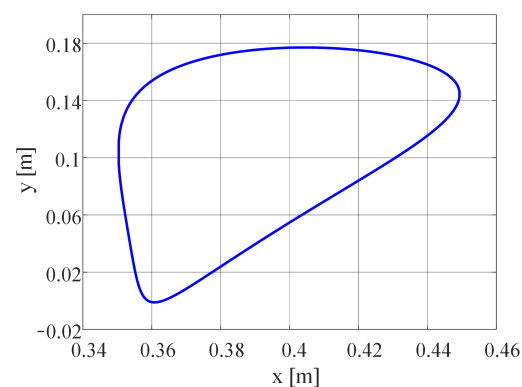
Figure 5. Path of the coupler point of the mechanism.

4.2. Constant Crank Velocity

The test consists of regulating the crank angular velocity of the mechanism at 5 rad/s (47.74 rpm) by means of the PID controller presented in [29]. The controller gains are given in Table 4. As observed in Figure 6a, the crank angular velocity is regulated with a maximum error of 0.02 rad/s, and the convergence time is 0.05 s (at 15°). In addition, Figure 6b shows that the velocity of the coupler point is variable all the time during the trajectory of the mechanism. As previously mentioned, this is the traditional control task for this mechanism; however, the coupler point is where the work is performed, so it is important to control its velocity at a desired value.
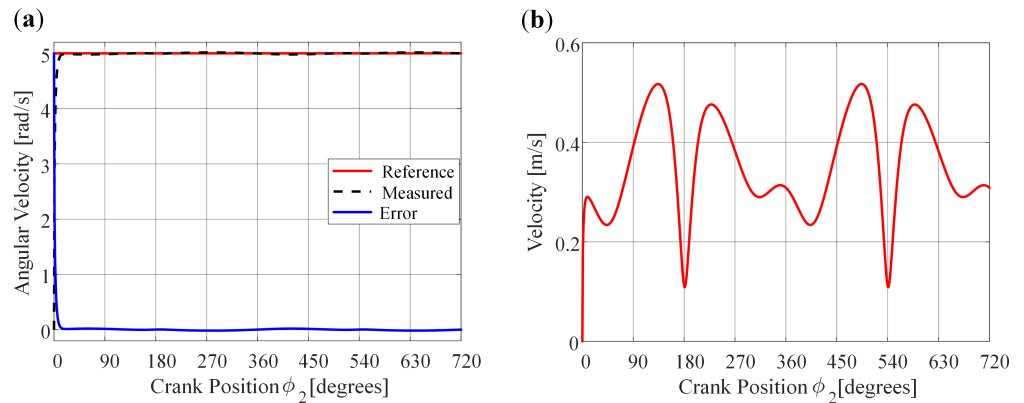

Figure 6. Simulation results of constant crank velocity with PID Control. (**a**) Crank angular velocity. (**b**) Coupler point velocity.

Table 4. Controller Gains.

Parameter	Value
K_p	3000
K_d	200
K_i	50
K_{p2}	10.8
K_{d2}	0
K_{i2}	100

4.3. Variable Input Velocity for Obtaining a Constant Output Velocity at the Coupler Point

This test is carried out to show that the proposed control scheme allows for indirect regulation of the velocity of the coupler point by fulfilling two requirements. Firstly, the reference crank velocity, obtained through the developed neural network, is close to the real value; additionally, the proposed control tracks this reference with minimal error. In this case, a velocity of 0.2 m/s is imposed for the coupler point. In Figure 7a it is noted that there is an excellent tracking of the desired trajectory, since the convergence time is 0.02 s (at 8°) and the maximum error is 0.07 rad/s. The previous result makes it possible to regulate the velocity of the coupler point at the desired value, as shown in Figure 7b. Note that the coupler point velocity error is less than 0.003 m/s and the convergence time is 0.02 s, which is consistent with that of the angular velocity of the crank presented in Figure 7a.
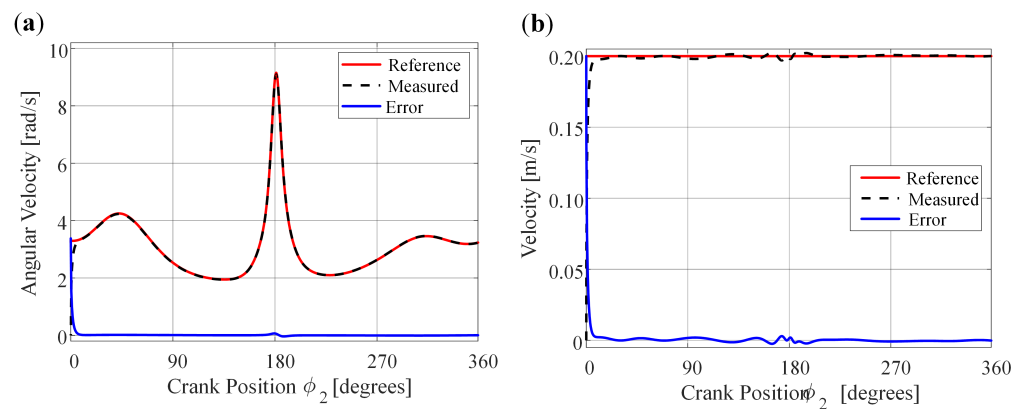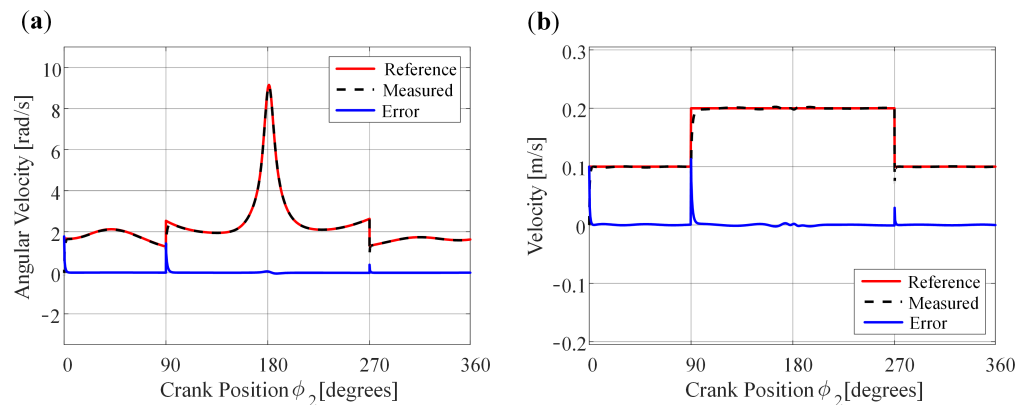
Figure 7. Variable input velocity for obtaining a constant output velocity at the coupler point. (**a**) Crank angular velocity. (**b**) Coupler point velocity.

4.4. Variable Input Velocity for Generating Two Different Output Velocities at the Coupler Point

In real applications, the coupler point is not required to carry out its entire travel with a constant velocity, but rather to have a specific velocity in the segment in which it performs the work and a different velocity for the return. For this reason, the experiment is carried out when a more complex velocity profile is imposed on the coupler point. As displayed in Figure 8a, the angular crank velocity reference has abrupt changes at 90° and 270°. These are needed to regulate the coupler point velocity to the conditions

$$V_Q = \begin{cases} 0.2 \text{ m/s} & 90° \leq \phi_2 < 270° \\ 0.1 \text{ m/s} & \text{otherwise.} \end{cases} \tag{47}$$

In Figure 8b, the coupler point velocity error is less than 0.003 m/s and the convergence time is 0.02 s, which are the same as the presented in Section 4.3 for the coupler point.
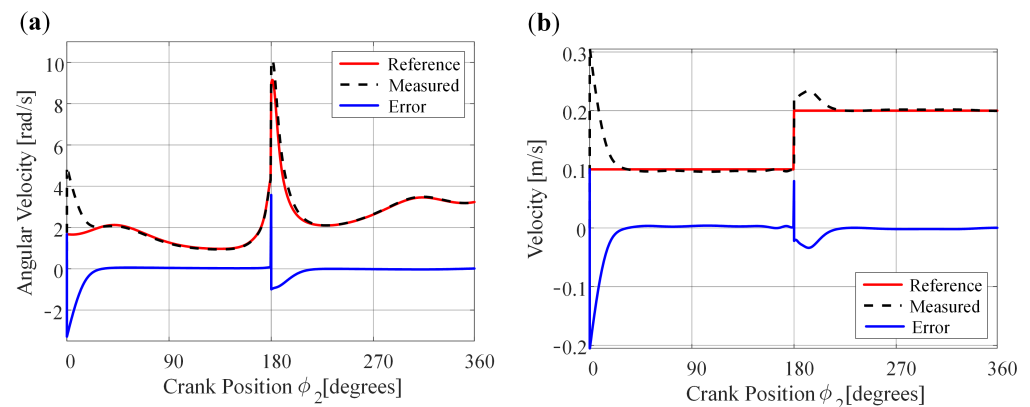

Figure 8. Variable input velocity for generating two different output velocities at the coupler point. (**a**) Crank angular velocity. (**b**) Coupler point velocity.

A more severe test is the one that implies that the velocity changes of the coupler point are where the control is most demanded, this happens when $\phi_2 = 180°$, which is where the most abrupt change would occur. In this test, the velocity profile that is imposed on the coupler point is

$$V_Q = \begin{cases} 0.2 \text{ m/s} & 180° \leq \phi_2 < 360° \\ 0.1 \text{ m/s} & \text{otherwise.} \end{cases} \tag{48}$$

Figure 9a shows the tracking of the crank velocity reference, this is fast and with minimum error. In Figure 9b, the change of velocity at the coupler point is presented. In this case, the convergence time is 0.0266 s (at 20°) and the maximum error is 0.03 m/s. It

can be emphasized that this would be the worst case for this mechanism; in spite of that, the system is controlled at the desired velocity at the specified points.

Figure 9. Variable input velocity for generating two different output velocities at the coupler point. (**a**) Crank angular velocity. (**b**) Coupler point velocity.

It is important to indicate that the saturation function was used in the simulation to prevent V_a from increasing to values that could cause some damage to the system; however, it was observed that in all the cases presented, such voltage did not reach the saturation limits. To exhibit this performance, Figure 10 shows the input voltage to the motor corresponding to the input profiles defined by (47) and (48), and the results are shown in Figures 8 and 9.
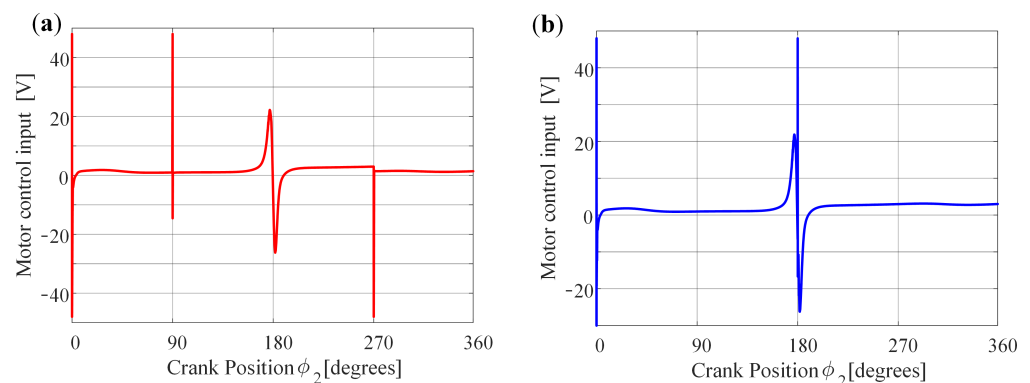
Figure 10. Variable input velocity for generating two different output velocities at the coupler point. (**a**) V_Q described in Equation (47). (**b**) V_Q described in Equation (48).

In summary, the designed controller achieved trajectory tracking with good performance both on tracking error and transient response. The proposed control scheme has a simple structure and low computational burden for real-time applications. In the case when more demanding performance is required, then the computational intelligence methods can be integrated with other high-performance algorithms such as the type-2 fuzzy presented in [25–27] which can deliver exact responses and robustness.

5. Conclusions

In this work, the problem of controlling a four-bar mechanism for the case of variable velocity of the crank is considered. To obtain the desired output motions for the coupler point, an indirect control is designed to estimate the reference values for the motor current to achieve trajectory tracking for each crank velocity profile. Furthermore, a neural network is introduced in the control scheme to solve the kinematic model of the mechanism to obtain the velocity reference. The controlled system is tested through simulations under several trajectories, obtaining excellent results. Further research will implement the four-bar

mechanism with the proposed controller using an optical encoder and or computer vision for the position feedback.

References

1. Tao, J.; Sadler, J. Constant speed control of a motor driven mechanism system. *Mech. Mach. Theory* **1995**, *30*, 737–748. [CrossRef]
2. Dulger, L.; Uyan, S. Modelling, simulation and control of a four-bar mechanism with a brushless servo motor. *Mechatronics* **1997**, *7*, 369–383. [CrossRef]
3. Li, Q.; Tso, S.; Guo, L.; Zhang, W. Improving motion tracking of servomotor-driven closed-loop mechanisms using mass-redistribution. *Mech. Mach. Theory* **2000**, *35*, 1033–1045. [CrossRef]
4. Wu, F.X.; Zhang, W.J.; Li, Q.; Ouyang, P.R. Integrated Design and PD Control of High-Speed Closed-loop Mechanisms. *J. Dyn. Syst. Meas. Control* **2002**, *124*, 522–528. [CrossRef]
5. Su, Y.; Sun, D.; Zheng, C. Nonlinear trajectory tracking control of a closed-chain manipulator. In Proceedings of the Fifth World Congress on Intelligent Control and Automation (IEEE Cat. No. 04EX788), Hangzhou, China, 15–19 June 2004; Volume 6, pp. 5012–5016. [CrossRef]
6. Lin, M.C.; Chen, J.S. Experiments toward MRAC design for linkage system. *Mechatronics* **1996**, *6*, 933–953. [CrossRef]
7. Gündoğdu, Ö.; Erentürk, K. Fuzzy control of a dc motor driven four-bar mechanism. *Mechatronics* **2005**, *15*, 423–438. [CrossRef]
8. Koca, G.O.; Akpolat, Z.H.; Özdemir, M. Type-2 Fuzzy Sliding Mode Control of A Four-Bar Mechanism. *Int. J. Model. Simul.* **2011**, *31*, 60–68. [CrossRef]
9. Hwang, C.L.; Kuo, C.Y. A stable adaptive fuzzy sliding-mode control for affine nonlinear systems with application to four-bar linkage systems. *IEEE Trans. Fuzzy Syst.* **2001**, *9*, 238–252. [CrossRef]
10. Koca, G.O.; Akpolat, Z.H.; Özdemir, M. Development of robust fuzzy control methods and their applications to a mechanical system. *Turk. J. Sci. Technol.* **2014**, *9*, 47–56.
11. Ren, Q.; Bigras, P. Design and implementation of model-free PID fuzzy logic control on a 4-bar parallel mechanism. In Proceedings of the 2015 IEEE International Conference on Advanced Intelligent Mechatronics (AIM), Busan, Republic of Korea, 7–11 July 2015; pp. 1647–1652. [CrossRef]
12. Zhang, Y.; Feng, C.; Li, B. PID Control of Nonlinear Motor-Mechanism Coupling System Using Artificial Neural Network. In *Advances in Neural Networks—ISNN 2006, Proceedings of the Third International Symposium on Neural Networks, Chengdu, China, 28 May–1 June 2006*; Wang, J., Yi, Z., Zurada, J.M., Lu, B.L., Yin, H., Eds.; Springer: Berlin/Heidelberg, Germany, 2006; pp. 1096–1103.
13. Lungu, R.; Sepcu, L.; Lungu, M. Four-Bar Mechanism's Proportional-Derivative and Neural Adaptive Control for the Thorax of the Micromechanical Flying Insects. *J. Dyn. Syst. Meas. Control* **2015**, *137*, 051005. [CrossRef]
14. Çakar, O.; Tanyıldızı, A.K. Application of moving sliding mode control for a DC motor driven four-bar mechanism. *Adv. Mech. Eng.* **2018**, *10*, 1687814018762184. [CrossRef]
15. Salah, M.; Al-Jarrah, A.; Tatlicioglu, E.; Banihani, S. Robust Backstepping Control for a Four-Bar Linkage Mechanism Driven by a DC Motor. *J. Intell. Robot. Syst.* **2019**, *94*, 327–338. [CrossRef]
16. Erenturk, K. Hybrid Control of a Mechatronic System: Fuzzy Logic and Grey System Modeling Approach. *IEEE/ASME Trans. Mechatronics* **2007**, *12*, 703–710. [CrossRef]
17. Al-Jarrah, A.; Salah, M.; Banihani, S.; Al-Widyan, K.; Ahmad, A. Applications of Various Control Schemes on a Four-Bar Linkage Mechanism Driven by a Geared DC Motor. *WSEAS Trans. Syst. Control* **2015**, *10*, 584–597.
18. Tutunji, T.A.; Salah, M.; Al-Jarrah, A.; Ahmad, A.; Alhamdan, R. Modeling and Identification of a Four-Bar Linkage Mechanism Driven by a Geared DC Motor. *Int. Rev. Mech. Eng.* **2015**, *9*, 296–306. [CrossRef]
19. İşbitirici, A.; Altuğ, E. Design and Control of a Mini Aerial Vehicle that has Four Flapping-Wings. *J. Intell. Robot. Syst.* **2017**, *88*, 247–265. [CrossRef]
20. Mohseni, S.A.; Duchaine, V.; Wong, T. A comparative study of the optimal control design using evolutionary algorithms: Application on a close-loop system. In Proceedings of the 2017 Intelligent Systems Conference (IntelliSys), London, UK, 7–8 September 2017; pp. 942–948. [CrossRef]
21. Rodríguez-Molina, A.; Villarreal-Cervantes, M.G.; Aldape-Pérez, M. Indirect adaptive control using the novel online hypervolume-based differential evolution for the four-bar mechanism. *Mechatronics* **2020**, *69*, 102384. [CrossRef]

22. Shi, K.; Liu, C.; Sun, Z.; Yue, X. Coupled orbit-attitude dynamics and trajectory tracking control for spacecraft electromagnetic docking. *Appl. Math. Model.* **2022**, *101*, 553–572. [CrossRef]

23. Liu, C.; Yue, X.; Shi, K.; Sun, Z. *Spacecraft Attitude Control: A Linear Matrix Inequality Approach*; Elsevier: London, UK, 2022. [CrossRef]

24. Perrusquía, A.; Flores-Campos, J.A.; Yu, W. Optimal sliding mode control for cutting tasks of quick-return mechanisms. *ISA Trans.* **2022**, *122*, 88–95. [CrossRef]

25. Hua, G.; Wang, F.; Zhang, J.; Alattas, K.A.; Mohammadzadeh, A.; The Vu, M. A New Type-3 Fuzzy Predictive Approach for Mobile Robots. *Mathematics* **2022**, *10*, 3186. [CrossRef]

26. Xu, S.; Zhang, C.; Mohammadzadeh, A. Type-3 Fuzzy Control of Robotic Manipulators. *Symmetry* **2023**, *15*, 483. [CrossRef]

27. Mohammadzadeh, A.; Sabzalian, M.H.; Ahmadian, A.; Nabipour, N. A dynamic general type-2 fuzzy system with optimized secondary membership for online frequency regulation. *ISA Trans.* **2021**, *112*, 150–160. [CrossRef]

28. Yan, H.S.; Yan, G.J. Integrated control and mechanism design for the variable input-speed servo four-bar linkages. *Mechatronics* **2009**, *19*, 274–285. [CrossRef]

29. Peón-Escalante, R.; Flota-Bañuelos, M.; Ricalde, L.J.; Acosta, C.; Perales, G.S. On the coupler point velocity control of variable input speed servo-controlled four-bar mechanism. *Adv. Mech. Eng.* **2016**, *8*, 1687814016678356. [CrossRef]

30. Flota-Bañuelos, M.; Peón-Escalante, R.; Ricalde, L.J.; Cruz, B.J.; Quintal-Palomo, R.; Medina, J. Vision-based control for trajectory tracking of four-bar linkage. *J. Braz. Soc. Mech. Sci. Eng.* **2021**, *43*. [CrossRef]

31. Goldstein, H.; Poole, C.; Safko, J. *Classical Mechanics*; Pearson Education: London, UK, 2011.

32. Haykin, S.S. *Neural Networks and Learning Machines*; Prentice Hall: London, UK, 2016.